Northumbria Research Link

Citation: Mora-Seró, Iván, Bisquert, Juan, Fabregat-Santiago, Francisco, Garcia-Belmonte, Germà, Zoppi, Guillaume, Durose, Ken, Proskuryakov, Yuri, Oja, Ilona, Belaidi, Abdelhak, Dittrich, Thomas, Tena-Zaera, Ramon, Katty, Abou, Lévy-Clément, Claude, Barrioz, Vincent and Irvine, Stuart (2006) Implications of the negative capacitance observed at forward bias in nanocomposite and polycrystalline solar cells. Nano Letters, 6 (4). pp. 640-650. ISSN 1530-6984

Published by: American Chemical Society

URL: http://dx.doi.org/10.1021/nl052295q <http://dx.doi.org/10.1021/nl052295q>

This version was downloaded from Northumbria Research Link: https://nrl.northumbria.ac.uk/id/eprint/19978/

Northumbria University has developed Northumbria Research Link (NRL) to enable users to access the University's research output. Copyright © and moral rights for items on NRL are retained by the individual author(s) and/or other copyright owners. Single copies of full items can be reproduced, displayed or performed, and given to third parties in any format or medium for personal research or study, educational, or not-for-profit purposes without prior permission or charge, provided the authors, title and full bibliographic details are given, as well as a hyperlink and/or URL to the original metadata page. The content must not be changed in any way. Full items must not be sold commercially in any format or medium without formal permission of the copyright holder. The full policy is available online: http://nrl.northumbria.ac.uk/policies.html

This document may differ from the final, published version of the research and has been made available online in accordance with publisher policies. To read and/or cite from the published version of the research, please visit the publisher's website (a subscription may be required.)

Northumbria University NEWCASTLE

CUSTOMER SERVICE EXCELLENCE CSE

UniversityLibrary

Observation of negative capacitance at forward bias as a common feature of nanocomposite and polycrystalline solar cells

Iván Mora-Seró*, Francisco Fabregat-Santiago, Germà Garcia-Belmonte, Juan Bisquert*

Departament de Ciències Experimentals, Universitat Jaume I, E-12080 Castelló, Spain.

Guillaume Zoppi†, Kent Durose, Yuri Proskuryakov

Departament of Physics, University of Durham, South Road, Durham DH1 3LE, UK.

†Now at NPAC, ~~University of~~ Northumbria, Ellison Building, Ellision Place, Newcastle upon Tyne, NE1 8ST

Ilona Oja, Abdelhak Belaidi, Thomas Dittrich

Hahn-Meitner-Institut, Glienicker Str. 100, D-14109 Berlin, Germany.

Ramón Tena-Zaera, Abbou Katty, Claude Lévy-Clément

LCMTR, Institut des Sciences Chimiques Seine Amont, CNRS, 2/8 rue Henri Dunant, 94320 Thiais, France.

Vincent Barrioz, Stuart J. C. Irvine

Department of Chemistry, Univeristy of Wales, Bangor, Gwynedd, LL57 2UW, UK.

*Corresponding authors. E-mail: sero@exp.uji.es, bisquert@uji.es

21 November 2005

Key words: Negative capacitance, impedance spectrometry, CdTe solar cells, *eta*-solar cells, solid state dye sensitized solar cell

Abstract

Four different types of solar cells have been characterized by impedance spectroscopy (IS): thin film CdS/CdTe devices, an extremely thin absorber (*eta*) solar cell made with microporous TiO_2/$In(OH)_xS_y$/PbS/PEDOT, an *eta*-solar cell of columnar ZnO/CdSe/CuSCN, and a solid state Dye Sensitized Solar Cell (DSSC) with Spiro-OMeTAD as transparent hole conductor. Each cell has been manufactured in a different laboratory and several samples of each type have been studied. Independent of the different origin, materials type (organic and inorganic), configuration and geometry of the cells studied, a negative capacitance behaviour has been observed in all of them at high forward bias. The experiments suggest a universality of the underlying phenomenon giving rise to this effect, constituting general behaviour for a broad range of solar cell devices. The deleterious effect of negative capacitance on the device performance is discussed by comparison of the obtained results with the behaviour of a conventional monocrystalline Si solar cell.

1. Introduction

The relatively high cost of the conventional Si monocrystalline solar cells has impelled, among others, the research in a second generation of thin film solar cells and cells based on nanocomposite concepts such as the DSSC[1,2] and the *eta*-solar cells.[3-5]

One of the most intensively studied types of thin film devices is the polycrystalline cell based on CdS/CdTe heterojunction, with a record efficiency of 16.5%.[6] Such devices are among the best candidates for terrestrial applications because of the relatively high efficiency, long-term stability ~~in~~ the performance, as well as a potential for low-cost production. Due to high absorption coefficient of CdTe (>104 cm-1) a layer of this material with a thickness of only about 2 μm is sufficient to absorb most of the useful part of the solar spectrum.[7,8]

On the other hand, other types of solar cells such as DSSC and *eta*-solar cells, based on alternative concepts, have also been thoroughly investigated with the aim to significantly decrease the production cost. The attractive side of such devices is a very thin absorber ~~–~~ a monolayer of dye for DSSC, or a semiconductor absorber layer with thickness of tenths of nanometers for *eta*-solar devices. In the later case, the absorber layer is situated in a nanometric or micrometric matrix allowing for a significant improvement in the light absorption due to the large effective area of the matrix. In these cells the photogenerated carriers are transferred into two different media. This fact permits to relax the high quality requirements of single crystal p-n junction devices enabling for low cost fabrication processes to be employed.

In the conventional DSSC the dye molecules are regenerated by a redox couple dissolved in an electrolyte. The use of an electrolyte causes problems in the process of its encapsulation and in the long-term stable performance. One of the options intended to avoid this problem is to substitute this liquid electrolyte by a transparent hole semiconductor, in our case Spiro-OMeTAD.[9] However, these solid state devices present a lower efficiency (~4.5%) in comparison with a liquid electrolyte DSSC (~10%). Those effects have been attributed to a higher recombination dynamics and low hole conductivity.[10]

The DSSC configuration has also inspired an alternative all-solid device, the *eta*-solar cell with a ~~semiconducting~~ extremely thin absorber sandwiched between two transparent, highly interpenetrated semiconductors of different kinds.[3-5] The highest efficiency demonstrated to date for this type of cell is 2.3% at 1/3 sun, obtained for an

eta-solar cell of columnar ZnO/CdSe/CuSCN,[11] which is one of the types of cells studied in this work. Additionally, an *eta*-solar cell made with microporous TiO_2/$In(OH)_xS_y$/PbS/PEDOT (~1% efficiency), has also been studied, presenting the interests of the use of an organic polymer as hole conductor, and the system of $In(OH)_xS_y$/PbS to improve the contact selectivity.

The potentialities of these four types of solar cells (in the presented and related configurations) stimulate an interest in the study of their AC behaviour, which can provide diverse information on device properties and performance. Impedance spectroscopy (IS) ~~–~~is a well known AC technique used for the study of electrochemical and solid state systems, and has been employed extensively ~~in~~ characterization of DSSC devices.[12-16] On the other hand the utilization of this technique in the characterization of solid-state solar cells is not ~~regular~~, although a few examples are shown in the literature.[17,18] In principle impedance spectroscopy measurements taken over a broad frequency range (mHz-MHz) may provide information on any system that is composed of a combination of interfacial and bulk transport processes, particularly on transport coefficients, recombination parameters and interfacial states in solar cells. It is this that makes the technique especially valuable for the characterization of the devices mentioned above, with a broader aim to find ~~the~~ ways to improve their performance and/or stability.

~~In~~ solar cells, AC measurements are normally used mostly in reverse conditions to obtain information on interfacial characteristics (admittance spectroscopy). In this work we have systematically analyzed ~~by~~ IS data over a wide range of biasing potential, both under reverse and forward bias, using dark and light conditions, for samples of four different types of solar cells: CdS/CdTe thin film solar cells, microporous TiO_2/$In(OH)_xS_y$/PbS/PEDOT, columnar ZnO/CdSe/CuSCN *eta*-solar cells, and a solid state DSSC with doped and undoped Spiro-OMeTAD as transparent hole conductor. In all ~~the~~ cases a strong negative capacitance has been observed at high forward bias conditions for low frequencies. Such behaviour is compared with the (positive) capacitance of a high performance silicon solar cell, and the implications of the negative capacitance effect, as well as possible interpretations, are discussed.

2. Experimental

The four solar cells analyzed ~~have been manufactured in~~ four different laboratories.

The CdS/CdTe solar cells were grown on 4×4 cm transparent conductive oxide (8 Ω/□) on glass by metal-organic chemical vapour deposition (MOCVD)[19] at the University of Wales, Bangor. The 120 nm CdS window layers were deposited at a substrate temperature of 300ºC using the organometallics dimethylcadmium (DMCd) and ditertiarybutylsulphide (DTBS) in the ratio 1:2. The 4 μm CdTe absorber layers were grown at 350ºC using DMCd and di-isopropyltelluride (DIPTe) in the ratio 1:1. The structures were activated using the well-known cadmium chloride ($CdCl_2$) treatment at Durham University using a 40nm thick chloride layer followed by annealing in nitrogen in a tube furnace at 420ºC for 18 min. The surfaces were etched using a solution of nitric and phosphoric acids (1% HNO_3, 70% H_3PO_4, 29% H_2O). Finally, gold contacts (~2.5 mm diameter dots) were evaporated onto the CdTe layer as back contacts, and In-Ga amalgam was applied to the front contact for electrical connection. Each device comprised 4 gold dots on a ~1 cm^2 area; the areas around dot contacts were not scribed to further define the region of charge collection.

The microporous TiO_2/$In(OH)_xS_y$/PbS/PEDOT:PSS *eta*-solar cells were produced at the Hahn-Meitner-Institute. Compact and microporous layers of TiO_2 were prepared by several dippings in a solution containing titanium isopropoxide onto glass substrates coated with conductive SnO_2:F and final firing at 500°C for 30 min. The $In(OH)_xS_y$ and PbS layers were deposited by the so-called SILAR (successive ion layer adsorption reaction) technique from 0.01 M $InCl_3$, 0.005 M $Pb(AcO)_2$ and 0.01 M Na_2S (pH = 7…8) precursor salt solutions and annealing in air at 200°C and 120°C, respectively. During the SILAR process, the samples were rinsed in water after each dipping step while the water was exchanged after each 5 dips. PEDOT:PSS layers were spin coated. The contact areas were defined by carbon ink back contacts. More details about TiO_2/$In(OH)_xS_y$/PbS/PEDOT:PSS eta-solar can be obtained in reference [20].

The columnar ZnO/CdSe/CuSCN *eta*-solar cells were performed at the LCMTR. A ZnO nanowires array was electrodeposited on conducting glass substrates, which were previously covered with a continuous ZnO sprayed layer. As a second step, a very thin CdSe coating was electrodeposited on ZnO nanowires, giving a ZnO/CdSe core-shell nanowires array. The empty space of the nanostructure was filled with chemically deposited CuSCN. To finish the *eta*-solar cell, a gold contact was vacuum evaporated on the CuSCN. More details about deposition processes are given in reference [11]. The studied samples were annealed in air at temperatures in the range of 350-400°C during 1

hour before CuSCN deposition.

The solid state DSSC with doped and undoped Spiro-Ometad as transparent hole conductor were made at the Imperial College of London. Measurements of samples where performed both at Imperial and at the University Jaume I, with a Potentiostat PGSTAT-30 equiped with an impedance analysis module. Details about preparation method of undoped samples are described in reference [10]. Doped samples were obtained by adding Sb to the OMeTAD solution prior to spin coating the sample.

In order to discuss the effect of the negative capacitance the IS results obtained for the above cells have been compared with those obtained for a Si monocrystalline solar cell supplied by BP-Solar Spain. From the original cell with a size of 12.5×12.5 cm^2 a smaller piece of 0.49 cm^2 was cut, in order to obtain a near homogeneous illumination on the entire cell surface.

Impedance measurements for all the cells, except for the CdS/CdTe solar cells, were carried out in the Universitat Jaume I with an Autolab PGSTAT-30 apparatus, equipped with a frequency analyser module. These measurements were made in the dark and under different illumination intensities employing a halogen lamp. Bias potentials in both reverse and forward ranges were applied, while 10 mV ac perturbation was used in impedance measurements with a frequency range from 1 MHz to 0.01 Hz. All the experiments were performed inside a Faraday cage or screened box.

Impedance measurements for the CdS/CdTe solar cells, were carried out at the University of Durham using a Solartron 1260 frequency response analyser and a 1296 dielectric interface. The amplitude of the ac signal was 40 mV for frequencies ranging from 3 MHz to 0.3 Hz at 20 values per decade. Similarly, experiments were repeated for different bias conditions. Light measurements were done under AM1.5 light spectrum at various intensities using on commercial ORIEL 300W solar simulator.

3. Solar cell capacitance: the standard model

For later reference we first analyze a high performance Si monocrystalline solar cell which follows in many respect the "ideal" model of a solar cell.[21] For the Si cell, the observed pattern of impedance Nyquist plot (Z'' vs Z') consists of a semicircle. It can be described by means of a simple equivalent circuit consisting of a series resistance R_S, connected in series with the parallel association of a resistance R_r, that should be identified with the recombination resistance, and the total capacitance of the cell C_{tot}.

The later is given by $C_{tot} = C_\mu + C_{dl}$, and represents the parallel association of the chemical capacitance, C_μ,[22] (also called diffusion capacitance), which originates from the increase of the minority carrier density, and the depletion-layer capacitance, C_{dl}, due to the space charge region.[17] It has been discussed elsewhere[22] that the chemical capacitance is a crucial element of solar cell devices, as it describes the splitting of Fermi levels (and hence, the photovoltage) for a given amount of photogenerated carriers.

When the cell is high forward-biased, its capacitance is mostly determined by the chemical capacitance, $C_{tot} \approx C_\mu$, which increases exponentially with the potential as

$$C_\mu \propto \exp(-qV_D / \eta kT) \quad (1)$$

where V_D is the potential difference in the parallel association of R_r with C_{dl}, if equivalent circuit terminology is used, q is the absolute value of the electron charge, η is the diode factor, k is the Boltzmann constant and T is the temperature. Here we define the forward bias as being a negative voltage, as is conventional in semiconductor device literature (the opposite convention is often used in the solar cell literature). The value C_{dl} can be expressed as $C_{dl}^{-2} = B(V_0 - V_D)$ where V_0 is the built-in potential and $B=2/qN\varepsilon_0\varepsilon_r$ with $N=N_AN_D/(N_A+N_D)$, where ε_0 is the permittivity of free space, ε_r the permittivity of the material, and N_A and N_B the doping concentration of *p* and *n* regions respectively.[21] For reverse bias the space charge region enlarges and C_μ diminishes and, consequently, $C_{tot} \approx C_{dl}$.

In Fig. 1, C_{tot} is plotted as function of V_D for different light illumination intensities. The behaviour of C_{tot} is divided in two regions, for high forward bias, $V_D <$ -0.4 V, the capacitance increases exponentially with the absolute V_D value as predicted in eq. (1), and its value is fixed by the bias potential independently of the applied illumination intensity. Fitting the data in this region, we have obtained the diode factor η=1.18, which is close to the ideal value η=1, as can expected from a high performance solar cell. For reverse bias the behaviour of C_{tot} with V_D has a much smaller gradient, and in this region $C_{tot} \approx C_{dl}$, so that the capacitance follows a Mott-Schottky plot. For a conventional DSSC with electrolyte an analogous behaviour to that shown in Fig. 1 has been observed, although with a higher value of η.[12,14,15]

4. General characteristics of the negative capacitance

The frequency-dependent capacitance is defined from the impedance, Z, as C=1/(iω

Z), where ω is the angular frequency of the ac perturbation. The impedance is separated in real and imaginary parts as Z = Z' + iZ'', and similarly, the complex capacitance is written as C = C' + iC'' where $C' = \mathrm{Re}(C)$. While most systems investigated by IS, can be described with (positive) resistors and capacitors, with Z'>0 and C'>0, respectively, as in the above mentioned Si solar cell, the appearance of negative capacitance is otherwise not uncommon. If the system is close to equilibrium, negative capacitance or resistance are not allowed, as such elements would upset the principles of thermodynamics. However, far from equilibrium, for example under strong steady-state bias, negative capacitance and resistance can be and are in fact found. Negative capacitance (or inductive behaviour) has been observed in a variety of electronic devices such as Schottky diodes,[23,24] short based p-n junctions,[25-27] polymer light-emitting diodes (PLEDs),[28-30] and DSSC.[31] The inductive feature of the ac impedance is also found in electrochemical measurements of electrocatalysis, electrodeposition and electro-dissolution.[32-40]

There are two main types of interpretations suggested for the negative capacitance. In the first one the inductive behaviour takes place when the current between two electronic reservoirs (such as oxidized and reduced ionic species in solution, or two bulk semiconductors connected by a quantum well) is governed by the occupation of an intermediate state, which decreases when the applied potential increases. An example is the electrocatalytic reaction $A \Leftrightarrow C$ controlled by an intermediate absorbed species B. From the analysis of Sadkowski[40,41] in terms of zeros and poles of the impedance, it can be infered that such electrocatalytic reactions, even those involving thermodynamically stable systems, display an inductive feature when the concentration of the adsorbed species decreases while the potential increases, contrary to the equilibrium isotherm, as a result of a significant charge-transfer current. In the case of Schottky diodes the negative capacitance was interpreted in terms of the loss of interface charge at occupied states bellow the Fermi level due to impact ionization.[24] In double-barrier resonant tunneling diodes (RTD) the quantum capacitance (similar to the chemical capacitance discussed above) was defined as the change of the charge stored in the quantum well with respect to a change of the potential in the RTD.[42] It was shown that the quantum capacitance becomes negative in the region of negative differential resistance due to decrease of electron charges in the quantum well at increasing forward bias.[42,43]

A different mechanism exists in short-base p-n junction which gives also a negative

capacitance.[25-27] Such effect appears as a consequence of the minority carrier depopulation at high forward bias, which induces a change of sign of the capacitance. The mechanism has been modeled regarding the series resistance corresponding to the neutral diode regions in addition to the diffusion (minority carrier) capacitance.[26]

5. Results and discussion

For the four types of solar cells studied in this work, a negative capacitance has been observed under dark conditions for high forward bias. An example of the IS results obtained for the CdS/CdTe solar cell is plotted in Fig. 2. In the low frequency range the Nyquist plot exhibits an arc with positive imaginary part of the impedance (note the minus sign in the imaginary part of the impedance axis). As a consequence the real part of the capacitance adopts negative values in this frequency range.

To obtain a broad view of the results obtained on the different types of solar cells described above, we compare in Fig. 3 the bias dependence of the capacitance with that already described for the Si monocrystalline solar cell. For the analyzed cells, and in contrast to the "ideal" behaviour of the Si sample, the device capacitance rises with increasing bias, reaches a maximum, and then rapidly decreases.

In Fig. 2, the frequency of transition between negative and positive imaginary parts of the impedance is displaced to higher values as the forward bias increases. The effect of this low frequency arc on the capacitance can be better observed in Fig. 4 for the four kinds of analyzed solar cells. Doped OMeTAD sample produced the same effect but it is not plotted for the sake of clarity. The real part of the capacitance of the device for high frequency increases as the frequency is decreased until a quasi-plateau region is attained. The value of the real part of the capacitance in this plateau region for high reverse bias (positive voltage) increases progressively as the reverse bias is reduced. As already discussed, in the standard model of a solar cell an exponential increase of the capacitance is expected with increase of the forward bias. However, instead of this behaviour, for the analyzed solar cells the apparition of the negative contribution at certain forward biases produces a pronounced decrease in the capacitance, giving raise to a dip in Abs(C') data in Fig. 4.

Fig. 5 shows the impedance spectra and capacitance versus frequency for a microporous TiO_2/$In(OH)_xS_y$/PbS/PEDOT *eta*-solar cell at different applied bias under 1 sun illumination (~~for~~ the same sample as in Fig. 4). ~~As it~~ can be seen from the

comparison of this data with the data in Fig. 4, the negative capacitance behaviour is enhanced under illumination. For example, the frequency of transition between positive and negative values of the real part of the capacitance at V=-0.5 V (forward bias), shifts by about two decades to higher frequency values due to photocarrier generation under illumination. Interestingly, for this sample under illumination a negative capacitance is also observed, for the reverse bias. Presumably this behaviour takes place due to the particularities of structure of this cell, for the other three types of cells do not show negative capacitance at reverse biases even under illumination. However, our results show that for all types of the cells studied here, the negative capacitance behaviour is enhanced under illumination in the same manner as for TiO_2/InS/PbS/PEDOT eta-solar cell described above.

We remark that in all the solar cells considered the resistance is positive as it is checked by current-voltage experiments, showing that for all the cells analyzed the current increases with the forward bias, indicating that the origin of the commented behaviour is purely capacitive.

A reduction in the capacitance of CdS/CdTe solar cells has also been observed by Friesen et al.,[44] and to explain this effect they employed the model of Niemegeers and Burgelman.[45] In this model the CdS/CdTe/Au contact behaves as a back to back diode. However, while that model can explain a reduction of the device capacitance for high forward bias, it is not capable to explain the negative capacitance observed in the present work.

In general the chemical capacitance in Eq. (1) relates to the approach of the quasi-Fermi level to conduction band level, both in thin film polycrystalline cells and DDSC, due to photogeneration of carriers.[22] As it is seen in Fig. 4, for the analyzed cells the appearance of the negative capacitance has a dramatic effect on the device capacity. Clearly, such behaviour implies that the overall capability of the device to store charge is strongly affected by the negative capacitance contribution, and by necessity this will also bear the effect on the device performance. The negative capacitance observed in the solar cells investigated here indicates a failure in the operation of these devices, due to some dynamic effect that prevents the accumulation of charge. While the phenomenon appears to be fairly general, further investigation is needed to determine the exact origin of the negative capacitance in the polycrystalline and nanocomposite solar cells. According to the first class of models discussed in Section 3, above, interfacial and

intergranular states could play an important role in the reported behaviour.

7. Conclusions

A negative capacitance behaviour has been observed ~~in~~ high forward bias in four different types of solar cells: ~~of~~ thin film CdS/CdTe devices, microporous TiO_2/$In(OH)_xS_y$/PbS/PEDOT and columnar ZnO/CdSe/CuSCN *eta*-solar cells, and a solid state DSSC with Spiro-OMeTAD as transparent hole conductor. In all ~~of the~~ cases the photogenerated carriers due to device illumination enhance this effect. The negative capacitance prevents these solar cells from obeying the "ideal" relationship consisting of an exponential increase of the number of carriers with respect to variation of quasi-Fermi level. Further investigation is needed to determine the exact origin of the negative capacitance in the solar cells studied to be able of surpassing this limitation to the efficiency.

Acknowledgements

The work was supported by Ministerio de Educación y Ciencia of Spain under project MAT2004-05168. Authors acknowledge BP Spain for provide the Si monocrystalline solar cell.

References

(1) O' Regan, B.; Grätzel, M. *Nature* **1991**, *353*, 737.

(2) Bisquert, J.; Cahen, D.; Rühle, S.; Hodes, G.; Zaban, A. *J. Phys. Chem. B* **2004**, *108*, 8106.

(3) Ernst, K.; Belaidi, A.; Könenkamp, R. *Semiconductor Science and Technology* **2003**, *18*, 63.

(4) Ernst, K.; Lux-Steiner, M. C.; Könenkamp, R. *European Photovoltaic Solar Energy Conference* **2000**, 63.

(5) Lévy-Clément, C.; Katty, A.; Bastide, S.; Zenia, F.; Mora, I.; Munoz-Sanjose, V. *Physica E* **2002**, *14*, 229.

(6) Wu, X.; Kane, J. C.; Dhere, R. G.; DeHart, C.; Albin, D. S.; Duda, A.; Gessert, T. A.; Asher, S.; Levi, D. H.; Sheldon, P. 17th European Photovoltaic Solar Energy, Conference and Exhibition, 2002, Munich.

(7) Romeo, A.; Terheggen, M.; Abou-Ras, D.; Bätzner, D. L.; Haug, F.-J.; Kälin, M.; Rudmann, D.; Tiwari, A. N. *Progress in Photovoltaics: Research and Applications* **2004**, *12*, 93–111.

(8) Durose, K.; Edwards, P. R.; Halliday, D. P. *Journal of Crystal Growth* **1999**, *197*, 733.

(9) Krüger, J.; Plass, R.; Cevey, L.; Piccirelli, M.; Grätzel, M.; Bach, U. *Appl. Phys. Lett.* **2001**, *79*, 2085.

(10) Fabregat-Santiago, F.; Bisquert, J.; Palomares, E.; Durrant, J. R. **2005**, in preparation.

(11) Lévy-Clément, C.; Tena-Zaera, R.; Ryan, M. A.; Katty, A.; Hodes, G. *Advanced Materials* **2005**, *17*, 1512.

(12) Kern, R.; Sastrawan, R.; Ferber, J.; Stangl, R.; Luther, J. *Electrochim. Acta* **2002**, *47*, 4213.

(13) Fabregat-Santiago, F.; García-Cañadas, J.; Palomares, E.; Clifford, J. N.; Haque, S. A.; Durrant, J. R.; Garcia-Belmonte, G.; Bisquert , J. *J. Appl. Phys.* **2004**, *96*, 6903.

(14) Fabregat-Santiago, F.; Bisquert, J.; Garcia-Belmonte, G.; Boschloo, G.; Hagfeldt , A. *Solar Energy Materials and Solar Cells* **2005**, *87*, 117.

(15) van de Lagemaat, J.; Park, N.-G.; Frank, A. J. *J. Phys. Chem. B* **2000**, *104*, 2044.

(16) Zhang, Z.; Zakeeruddin, S. M.; O'Regan, B. C.; Humphry-Baker, R.; Grätzel, M. *J. Phys. Chem. B* **2005**, *109*, 21818.

(17) Bisquert, J.; Fabregat-Santiago, F.; Mora-Seró, I.; Garcia-Belmonte, G. "20th European Photovoltaic Solar Energy Conference and Exhibition", 2005, Barcelona.

(18) Kumar, R. A.; Suresh, M. S.; Nagaraju, J. *IEEE Transactions on Electron Devices* **2001**, *48*, 2177.

(19) Irvine, S. J. C.; Hartley, A.; Stafford, A. *Journal of Crystal Growth* **2000**, *221*, 117.

(20) Bayon, R.; Musembi, R.; Belalidi, A.; Bär, M.; Guminskaya, T.; Lux-Steiner, M.-C.; Dittrich, T. *Solar Energy Materials and Solar Cells* **2005**, *89*, 13.

(21) Sze, S. M. *Physics of Semiconductor Devizes*, 2nd ed.; John Wiley and Sons: New York, 1981.

(22) Bisquert, J. *Phys. Chem. Chem. Phys.* **2003**, *5*, 5360.

(23) Wang, C. D.; Zhu, C. Y.; Zhang, G. Y.; Shen, J.; Li, L. *IEEE Transactions on Electron Devices* **2003**, *50*, 1145.

(24) Wu, X.; Yang, E. S.; Evans, H. L. *Journal of Applied Physics* **1990**, *68*, 2846.

(25) Lindmayer, J.; Wrigley, C. Y. in *Fundamentals of Semiconductor Devices*; Van Nostrand: New York, 1965; pp 237.

(26) van den Biesen, J. J. H. *Solid-State Electronics* **1990**, *33*, 1471.

(27) Laux, S. E.; Hess, K. *IEEE Transactions on Electron Devices* **1999**, *46*, 396.

(28) Martens, H. C. F.; Huiberts, J. N.; Blom, P. W. M. *Appl. Phys. Lett.* **2000**, *77*, 1852.

(29) Hulea, I. N.; van der Scheer, R. F. J.; Brom, H. B.; Langeveld-Voss, B. M. W.; van Dijken, A.; Brunner, K. *Appl. Phys. Lett.* **2003**, *83*, 1246.

(30) Gommans, H. H. P.; Kemerink, M.; Andersson, G. G.; Pijper, R. M. T. *Phys. Rev. B* **2004**, *69*, 155216.

(31) Kron, G.; Egerter, T.; Werner, J. H.; Rau, W. *J. Phys. Chem. B* **2003**, *107*, 3556.

(32) Keddam, M.; Mattos, O. R.; Takenouti, H. *J. Electrochem. Soc.* **1981**, *128*, 257.

(33) Bai, L.; Conway, B. E. *Electrochim. Acta* **1993**, *38*, 1803.

(34) Wu, X.; Ma, H.; Chen, S.; Xu, Z.; Sui, A. *J. Electrochem. Soc.* **1999**, *146*, 1847.

(35) Hens, Z.; Gomes, W. P. *J. Phys. Chem. B* **2000**, *104*, 7725.

(36) Lauvstad, G. O.; Tunold, R.; Sunde, S. *J. Electrochem. Soc.* **2002**, *149*, E497.

(37) Gabrielli, C.; Keddam, M.; Minouflet-Laurent, F.; Ogle, K.; Perrot, H. *Electrochim. Acta* **2003**, *48*, 1483.

(38) Koper, M. T. M. *Adv. Chem. Phys.* **1996**, *92*, 1.

(39) Berthier, F.; Diard, J. P.; Montella, C. *Electrochimica Acta* **1999**, *44*, 2397.

(40) Sadkowski, A. *Journal of Electroanalytical Chemistry* **1999**, *465*, 119.

(41) Sadkowski, A. *Electrochim. Acta* **2004**, *49*, 2259.

(42) Hu, Y.; Stapleton, S. P. *Applied Physics Letters* **1993**, *58*, 167.

(43) Hu, Y.; Stapleton, S. P. *IEEE J. Q. Electron.* **1993**, *29*, 327.

(44) Friesen, G.; Dunlop, E. D.; Wendt, R. *Thin Solid Films* **2001**, *387*, 239.

(45) Niemegeers, A.; Burgelman, M. *Journal of Applied Physics* **1997**, *81*, 2881.

Figure Captions

Fig. 1: BP Si monocrystalline solar cell, device capacitance C_{tot} as function of device potential, V_D, for different light intensities, solid line represents the fit of C_μ in the potential region where it is dominant.

Fig. 2: Impedance spectra for CdS/CdTe solar cell at two different forward bias in dark conditions. The frequency range employed in the measurement was 1 MHz – 0.1 Hz.

Fig. 3: Real part of the capacitance for the solar cells analyzed under dark for a frequency of 10 Hz. The fit of C_{tot} for the Si monocrystalline solar cell under dark, Fig 4, is also included for comparison.

Fig. 4: Absolute value of the real part of the capacitance for the solar cells analyzed under dark conditions. The minimum observed at intermediated frequencies indicates the transition frequency between positive (high frequency) and negative capacitance (low frequency)..

Fig. 5: (a) Impedance spectra for $TiO_2/In(OH)_xS_y/PbS/PEDOT$ solar cell at different applied bias under 1 sun illumination. The frequency range employed in the measurement was 1 MHz – 0.1 Hz (0.01 Hz for TiO_2/dye/OMeTAD cells). **(b)** Zoom of the impedance spectra shown in (a). **(c)** Absolute value of the real part of the capacitance for TiO_2/InS/PbS/PEDOT solar cell under dark conditions. The minimum observed at intermediated frequencies indicates the transition frequency between positive (high frequency) and negative capacitance (low frequency).

Fig. 1

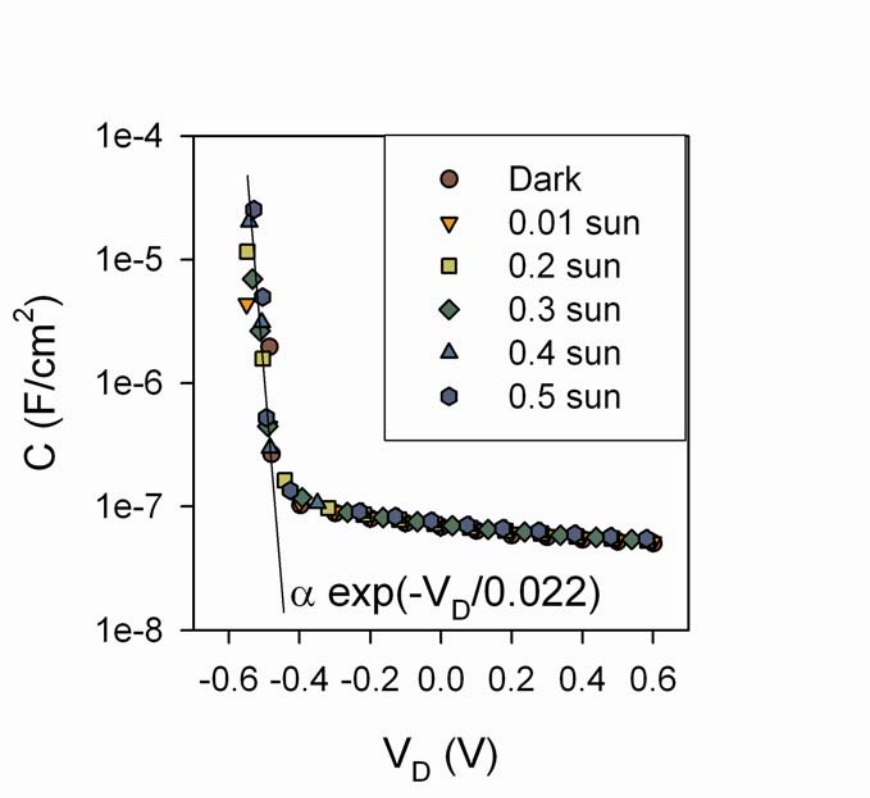
1e-4
1e-5
1e-6
1e-7
1e-8
C (F/cm^2)
Dark
0.01 sun
0.2 sun
0.3 sun
0.4 sun
0.5 sun
α exp(-V_D/0.022)
-0.6 -0.4 -0.2 0.0 0.2 0.4 0.6
V_D (V)

Fig. 2

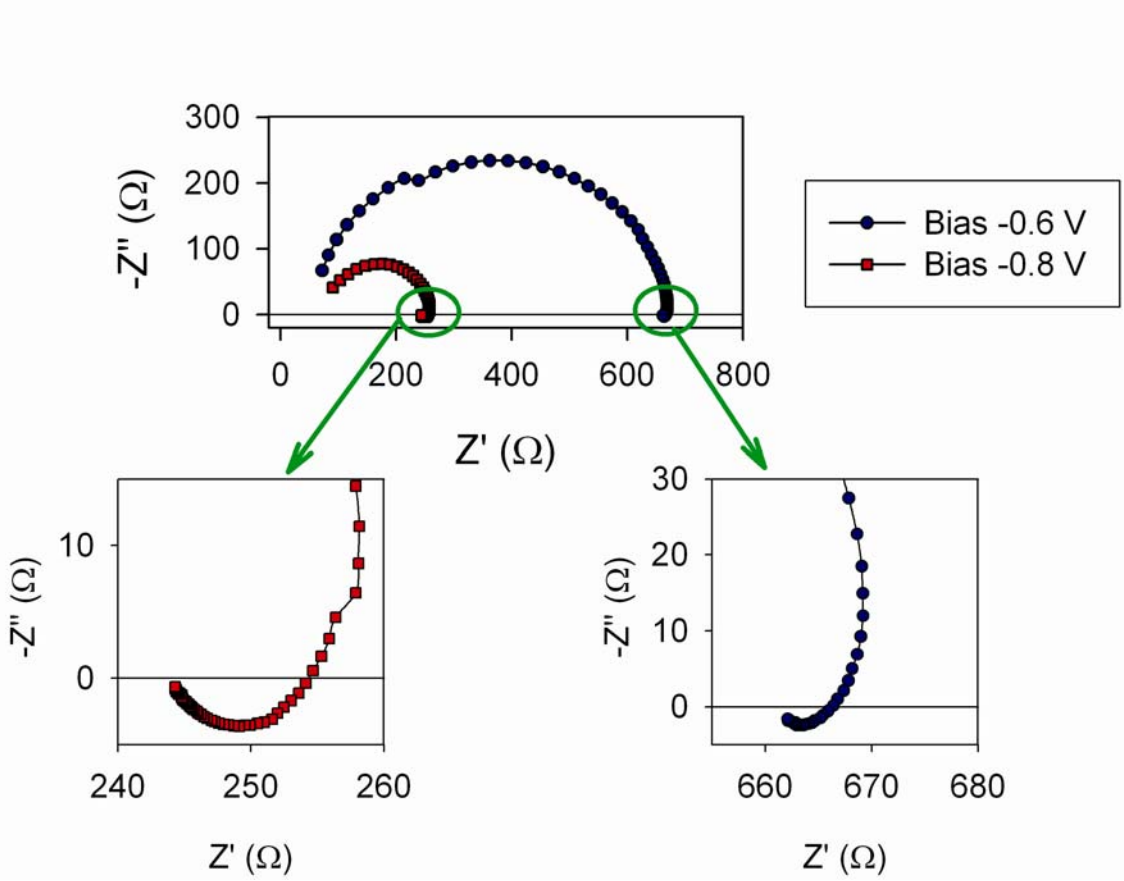
300
200
100
0
-Z'' (Ω)
0
200
400
600
800
Z' (Ω)
Bias -0.6 V
Bias -0.8 V
10
0
-Z'' (Ω)
240
250
260
Z' (Ω)
30
20
10
0
-Z'' (Ω)
660
670
680
Z' (Ω)

Fig. 3

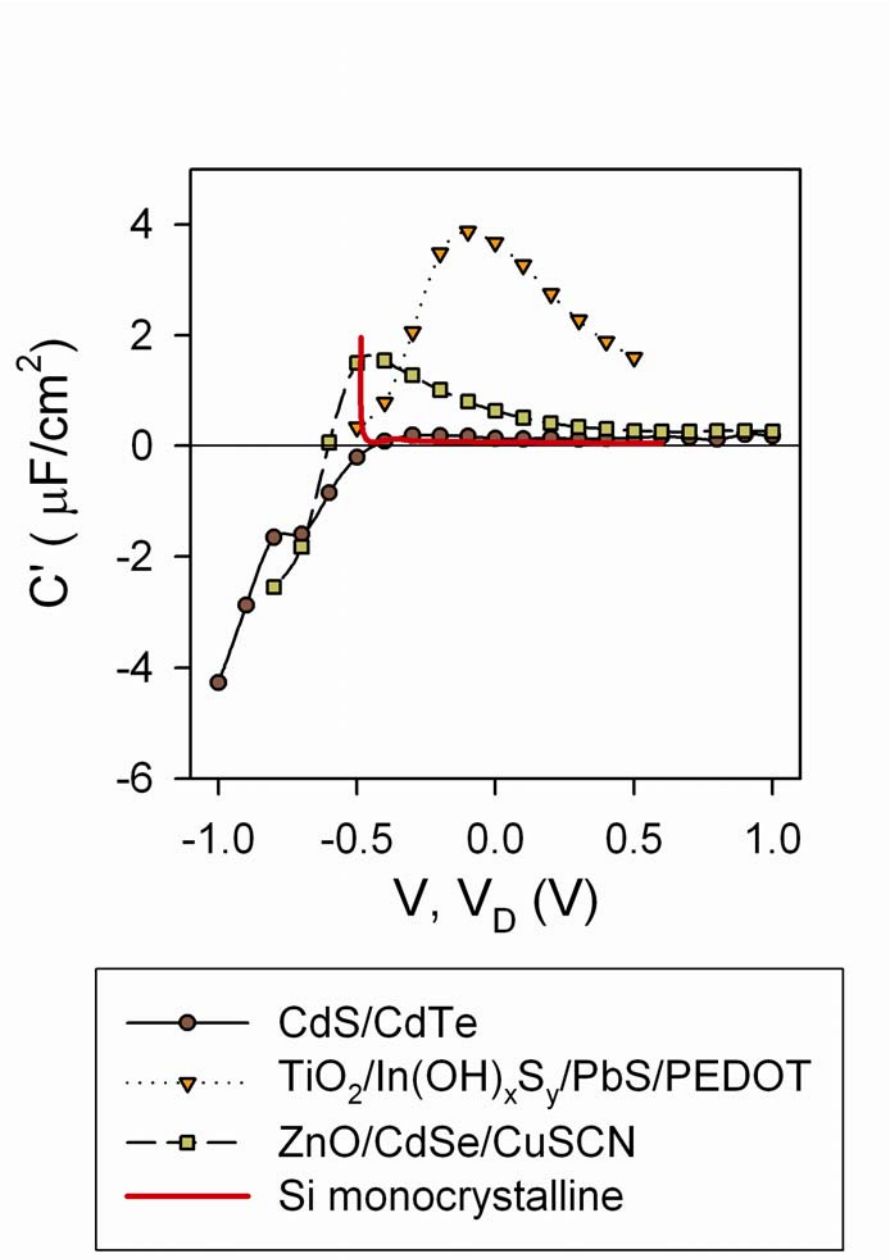
C' (μF/cm²)
4
2
0
-2
-4
-6
-1.0
-0.5
0.0
0.5
1.0
V, V_D (V)
CdS/CdTe
TiO2/In(OH)xSy/PbS/PEDOT
ZnO/CdSe/CuSCN
Si monocrystalline

Fig. 4

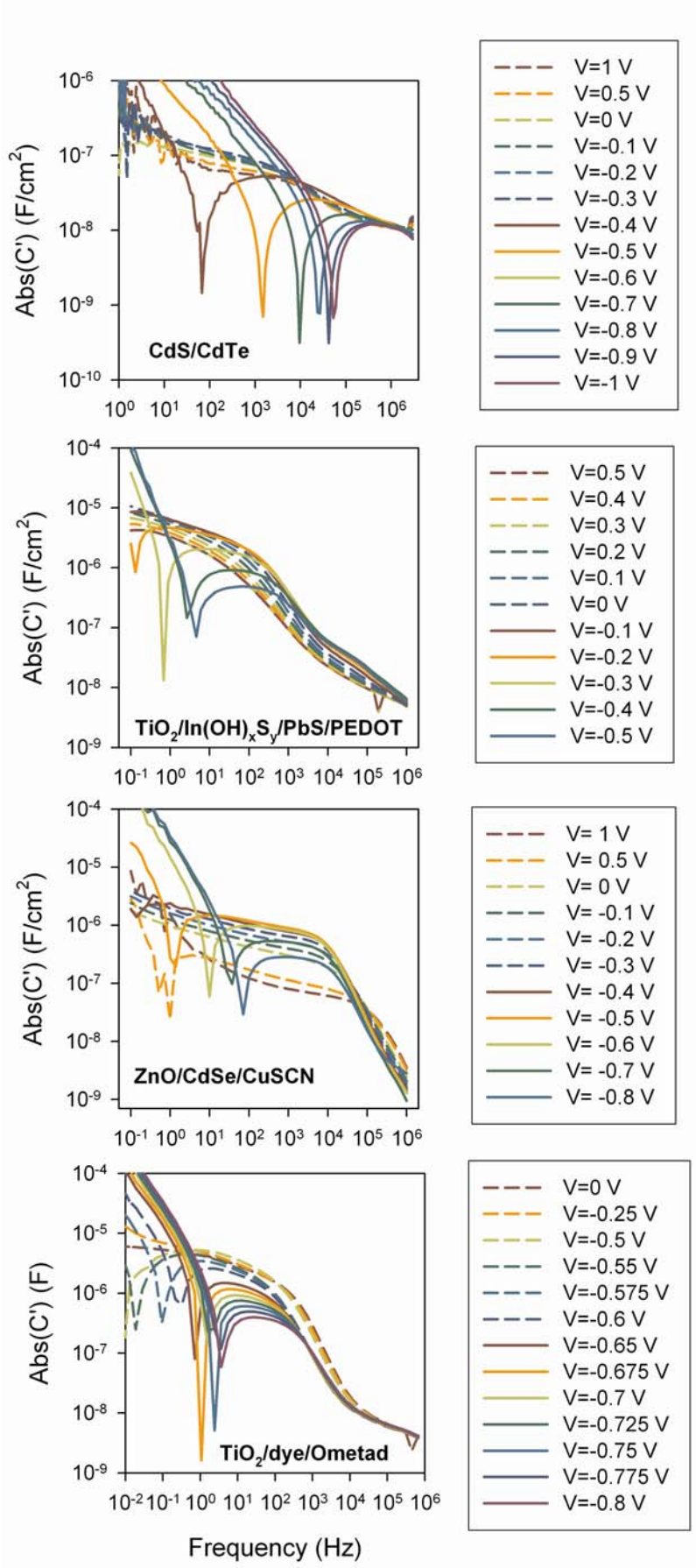
Abs(C') (F/cm²)
CdS/CdTe
V=1 V
V=0.5 V
V=0 V
V=-0.1 V
V=-0.2 V
V=-0.3 V
V=-0.4 V
V=-0.5 V
V=-0.6 V
V=-0.7 V
V=-0.8 V
V=-0.9 V
V=-1 V
Abs(C') (F/cm²)
TiO2/In(OH)xSy/PbS/PEDOT
V=0.5 V
V=0.4 V
V=0.3 V
V=0.2 V
V=0.1 V
V=0 V
V=-0.1 V
V=-0.2 V
V=-0.3 V
V=-0.4 V
V=-0.5 V
Abs(C') (F/cm²)
ZnO/CdSe/CuSCN
V= 1 V
V= 0.5 V
V= 0 V
V= -0.1 V
V= -0.2 V
V= -0.3 V
V= -0.4 V
V= -0.5 V
V= -0.6 V
V= -0.7 V
V= -0.8 V
Abs(C') (F)
TiO2/dye/Ometad
V=0 V
V=-0.25 V
V=-0.5 V
V=-0.55 V
V=-0.575 V
V=-0.6 V
V=-0.65 V
V=-0.675 V
V=-0.7 V
V=-0.725 V
V=-0.75 V
V=-0.775 V
V=-0.8 V
Frequency (Hz)

Fig. 5

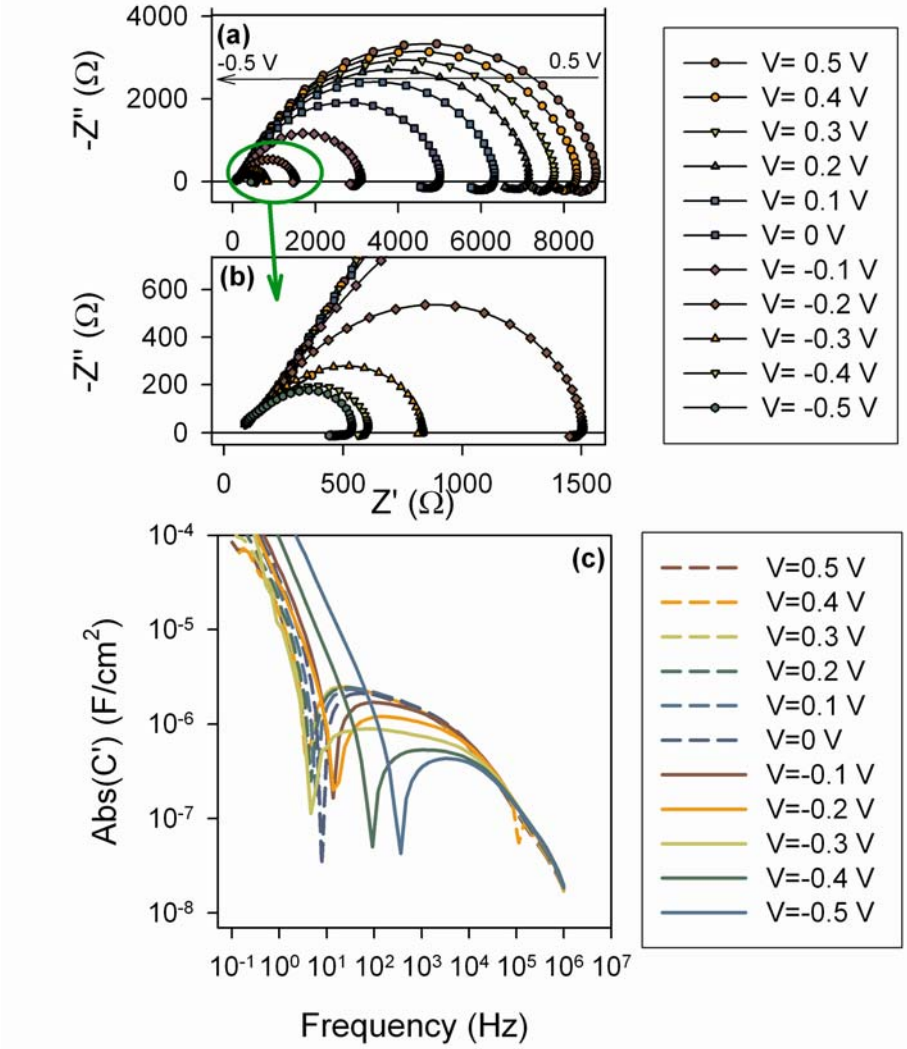
(a)
-0.5 V
0.5 V
-Z'' (Ω)
4000
2000
0
0
2000
4000
6000
8000
(b)
600
400
200
0
0
500
1000
1500
Z' (Ω)
V= 0.5 V
V= 0.4 V
V= 0.3 V
V= 0.2 V
V= 0.1 V
V= 0 V
V= -0.1 V
V= -0.2 V
V= -0.3 V
V= -0.4 V
V= -0.5 V
(c)
Abs(C') (F/cm²)
10⁻⁴
10⁻⁵
10⁻⁶
10⁻⁷
10⁻⁸
10⁻¹ 10⁰ 10¹ 10² 10³ 10⁴ 10⁵ 10⁶ 10⁷
Frequency (Hz)
V=0.5 V
V=0.4 V
V=0.3 V
V=0.2 V
V=0.1 V
V=0 V
V=-0.1 V
V=-0.2 V
V=-0.3 V
V=-0.4 V
V=-0.5 V